Lasers in Manufacturing Conference 2017

Excimer lasers micromachining of low density inorganic material

I. Geoffray*, R. Bourdenet, C. Chicanne, M. Theobald

CEA, Centre de Valduc, 21120 Is Sur Tille, France

Abstract

CEA designs, studies and manufactures targets dedicated to laser experiments. A target is composed of a wide range of materials that are often thin, fragile and requiring high-level micro-technology means. In this context, laser micro-machining processes offer reliable and accurate solutions, able to fulfill demanding specifications.
This presentation deals with tantalum oxide aerogel (Ta_2O_5) machining. This inorganic nanoporous material, combining a high-Z element and a quite low density (0.5 $g.cm^{-3}$), is of great interest for laser experiments. This paper shows how we achieved to shape this material with excimer laser, in UV nanosecond regime.
The first part of the study consisted in comparing the ablation rates obtained with ArF or KrF lasers, revealing slight differences of the material behaviour and phenomena like incubation or saturation. Then parametric optimization has been performed, and will be described, resulting in sub-millimetric 3D shapes (example of high-aspect ratio holes).

Keywords: excimer laser ; pulsed laser ; micro-machining ; target

1. Introduction

Over the past 20 years, excimer lasers have demonstrated their ability for material processing. Many authors report efficient surface ablation of polymers, glasses and ceramics (Ihleman, 1993, Ampere, 2007, Desbien, 2007): due to its high photon energy, excimer radiation is efficiently absorbed in a very thin surface layer, inducing an effective material removal. Consequently, excimer laser can ablate directly, in a one-step process.

* Corresponding author.
E-mail address: Isabelle.geoffray@cea.fr.

However, most publications mention surface micromachining of structures of less than 500 µm high. In this paper, we attempted to go further, with the evaluation of this micromachining technique for the fabrication of millimetric elements. For that, we focused on a material of interest for laser-plasma experiments: a tantalum oxide (Ta_2O_5) aerogel. The main advantages of this material lie both in its high Z and its nanostructure. Due to its porous structure, densities as low as 0.5 g/cc can be obtained, and volumes exceeding 1 cm^3 are currently available. However, the main drawback comes from the brittle behavior of Ta_2O_5 aerogels. From this point of view, a non-contact method like laser micromachining may be a suitable alternative to conventional method (diamond turning and milling).

The choice of excimer lasers has been driven by the dielectric behavior of Ta_2O_5 aerogels. The material bandgap (3.9 eV – Ambreen, 2014) can indeed be overcome by the excimer photon energy (5 eV for KrF laser and 6.4 eV for ArF laser). Unfortunately, very few data can be found in the literature about thermal and optical behavior features of Ta_2O_5 aerogels, compromising the understanding of Ta_2O_5 aerogel ablation.

A first part of this study treats of a phenomenological characterization of the ablation process, with the measurements of etch rates under excimer beam exposition. This allowed us to determine characteristic data of ablation. Two different measurement methods have been compared, in static or dynamic mode.
A second part details a specific parametric study, for the manufacturing of millimetric tubes from bulk samples of Ta_2O_5. The difficulty arises from the "laser milling" of the inner part (inner diameter: about 1.2 mm), inducing taper defects due to the beam focalization angle. So various operating parameters have been investigated and their effect on the holes geometry analyzed. The final goal was (a) to determine the best set of parameters, corresponding to the better cylindrical shape, (b) to estimate process limits in terms of taper defect and maximum achievable depth.

2. Experimental set-up

2.1. Laser micromachining systems

Our excimer workstations enable 2D and 3D processing (Bourdenet, 2015). They include Coherent lasers (COMPexPro serie) operating at 248 nm (argon-fluoride) or 193 nm (krypton-fluoride). Pulse duration is 20 ns FWHM and pulse energies reach 450 mJ. Repetition rates are adjustable between 1 Hz and 50 Hz.
Spatially speaking, the high M^2 factor of delivered beams makes them unsuitable for focusing on small area. But, in that case, their low spatial coherence is an advantage, allowing the use of projection optics. Thus, with the addition of masks and de-magnifying optics, optical benches have been configured for a traditional mask-projection technique. This way, masks are imaged on the sample with a demagnification factor of 1/8 or 1/15 (according to the chosen optics). So beams shapes can be adapted to the requested machining geometry, and are devoid of aberrations or diffraction effects.
Masks are manufactured by laser micromachining or by EDM techniques, and consist in pinholes (with various shape and dimensions) machined in metal foils. The advantages of such binary masks are their long lifetime and their high spatial contrast. They are also well adapted to our machining method, usually by spot writing.
Spot writing is performed by displacement of the sample with fixed and focused laser beam. Workpieces are positioned on a motorized stage that can rotate (Θ) and translate in all three axes (X-Y-Z) through a computerized controller. Stages resolution, repeatability and accuracy are currently less than 1 µm.
To complete the laser workstations description, CCD cameras are mounted on top of objective lenses to monitor the machining process and spot the beam.

2.2. Material synthesis

Tantalum oxide aerogels are obtained by a sol-gel method (Holland, 2014, Frederick, 2009). A tantalum precursor (tantalum ethoxide) is dissolved in a solvent (ethanol), combined to a catalyst mixture and poured into test tubes, where chemical reactions of hydrolysis and condensation take place, leading to the formation of a polymeric network (gel). After a maturation phase, gels are supercritically dried under ethanol atmosphere. Finally, a sintering step sets the density and improves the samples mechanical hardness.
After this process, centimetric samples are available.

3. Material response under excimer beam exposition

3.1. Laser-matter interaction

As it is well known (Lippert, 2004, Ampere, 2007), laser ablation in the UV range is the consequence of two phenomena in competition:

- photochemical ablation, where electronic excitation results in direct bond dissociation,
- photothermal ablation, where the electronic excitation is thermalized on a picosecond timescale and then results in thermal bond breaking.

Both happen simultaneously and can affect the etch rate. Classically, the comparison of L_o and L_e (resp. optical and thermal penetration depths) allows classifying materials behaviour and concluding if materials are suited to be micro-machined by excimer laser. In the case of Ta_2O_5 aerogels, this analysis is not directly possible because of the lack of basic optical and thermal material characterizations. However, we can consider the photochemical ablation process according to the following equation (derived from Beer-Lambert law):

$$d(F) = \frac{1}{\alpha_{eff}} \ln\left(\frac{F}{F_{th}}\right)$$

Where α_{eff} is the effective absorption coefficient (inverse of the optical penetration depth), F the incident fluence (J/cm^2) and F_{th} the ablation threshold fluence (J/cm^2).
This formula highlights two characteristic data of the laser photochemical ablation that are α_{eff} and F_{th}. In our case, they can be compared to values usually obtained for well-known processed materials with excimer lasers (polymers, glasses and ceramics).

3.2. Static etch rate

For this measurement, impacts have been performed at the surface of a flat Ta_2O_5 sample. This sample was positioned at the focal plane and exposed to a square spot (50 µm wide) at increasing fluence. Impacts depths have been measured by confocal microscopy, enabling surface scanning and profiles extraction.

The etch rate is defined as the depth of the ablation cratered after one pulse at a given fluence. The main issue with this approach comes from the feasibility of the depth measurement of shallow craters. That is why we preferred the accumulation of several pulses: a number N of 5 and 10 pulses has been tested. For the etch rate determination, the penetration depth is then divided by N (implying that each pulse contributes equally to the ablation depth). Measurements are given below for ArF laser (Fig 1a) or KrF laser (Fig 1b).

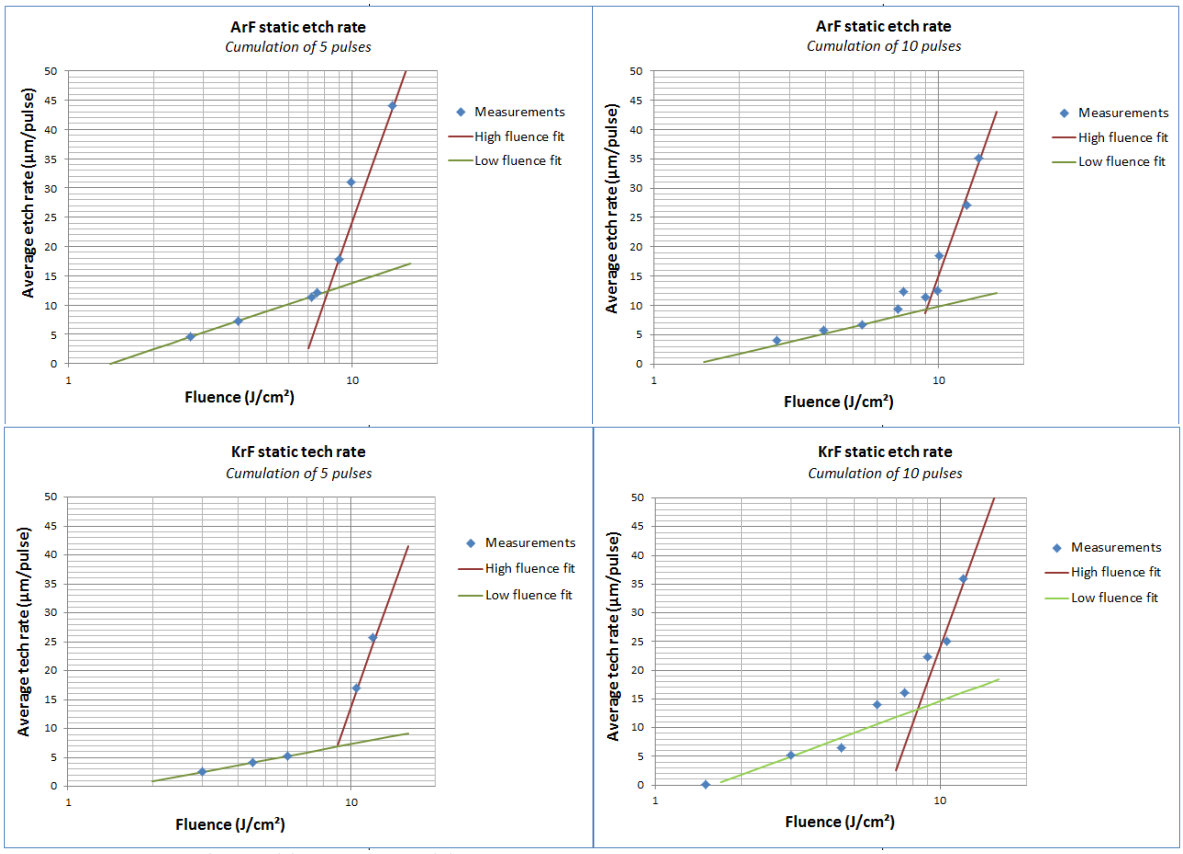

Fig. 1. Static etch rate vs fluence (a) with ArF laser; (b) with KrF laser. For each case, 5 or 10 pulses have been accumulated.

Fig 1 shows two different fluence ranges, as it has already been observed for materials like polymers or glasses (Dyer, 1996, Lippert, 2004, Urecht, 2010):

- a low fluence range, where ablation threshold is defined,
- a high fluence range, featuring an increased slope due to a more efficient material ablation.

Ablation parameters (α_{eff} and F_{th}) can be experimentally determined for each range from a linear interpolation of the log-scale curves:

Table 1. Static ablation parameters of Ta_2O_5 aerogel

λ (nm)	Number of cumulated pulses	Low fluence range		High fluence range	
		α_{eff} (μm^{-1})	F_{th} (J/cm^2)	α_{eff} (μm^{-1})	F_{th} (J/cm^2)
248	5	0.250	1.6	0.016	6
	10	0.125	1.6	0.016	6.7
193	5	0.143	1.4	0.016	6.7
	10	0.200	1.4	0.016	7.8

If we compare our experimental data with those of other materials (Lippert, 2004, Ampere, 2007), substantial differences appear:

- α_{eff} values are far lower than those observed for polymers (resp. > 5 μm^{-1} and > 1.5 μm^{-1} in low and high fluence ranges) or consumer glasses (> 2 μm^{-1} in low fluence range)
- Conversely, F_{th} are higher than those of polymers (resp. < 100 mJ/cm^2 and < 0.5 J/cm^2 in low and high fluence range) and a number of glasses (BK7 or borosilicate glasses). Only a few glasses (pyrex glass for example) feature similar threshold (1.6 J/cm^2).

That implies that Ta_2O_5 aerogel needs a much higher energy density to be ablated, and features longer optical penetration depths (approx. 5 µm at low fluence and 60 µm at high fluence) compared to polymers (usually < 1 µm). That probably ranks the material among weak absorbers.

We observed also that α_{eff} values at low fluence are greater than those obtained at high fluences. This can be related to incubation effects (i.e. physical or chemical modifications of the material by the first few pulses). This effect often results in an increase of the absorption coefficient at the irradiation wavelength (Urech, 2010). In our case, incubation effect probably stretches over the first 5 pulses for KrF laser, and over more 10 pulses for ArF laser.

Finally, both wavelengths led to similar results. Thus in the following of this work we implemented only the ArF laser, usually leading to better surface quality than KrF laser.

4. Dynamic etch rates measurement

In order to characterize the material response in a configuration closer to the process (i.e. for tube fabrication), we performed larger impacts (800 µm in diameter) in a thin sample of Ta_2O_5, in one cut, at increasing fluence.

For that, we programmed concentric circular motions (XY circular interpolation) of a thin sample, without any spatial overlap between two adjacent circles. The spot was circular (130 µm in diameter), the repetition rate was fixed at 50 Hz and the linear velocity at 5 mm/min.

As expected, penetration depth increases with fluence (Fig. 2a). A saturation effect is slightly observable above a pulse energy of 200 mJ.

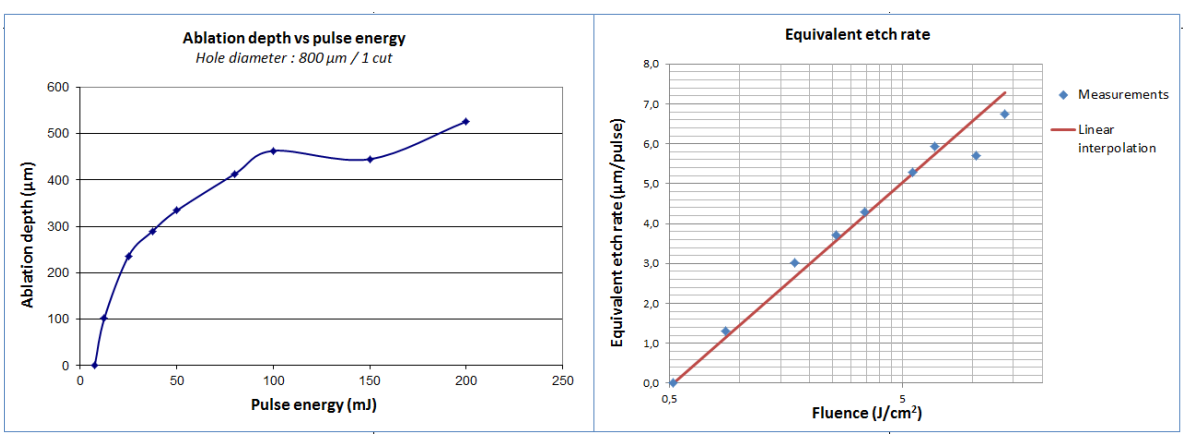

Fig. 2. Dynamic penetration measurements vs fluence (ArF laser) (a) penetration depth; (b) etch rate

To interpret curve in Fig. 2a and extract an etch rate, we need to know the number of pulses N impacting each point of the ablated area. For that we approximated the beam transverse profile to tophat, which seems reasonable for an excimer laser beam (high M^2). In that case, N is directly proportional to the laser repetition rate (f), the beam diameter (D) and the linear velocity (v), according to the following formula:

$$N_{Tophat} = \frac{f}{v} D$$

In our conditions, N= 84 pulses. Dividing the ablation depth by 84, we obtained the averaged etch rate plotted in Fig 2b as a function of fluence. Again, we obtained in log scale a linear function corresponding to the following ablation parameters:

Table 2. Dynamic ablation parameters of Ta_2O_5 aerogel

λ (nm)	Number of cumulated pulses	Low fluence range	
		α_{eff}^{eq} (µm^{-1})	F_{th} (J/cm^2)
193	84	0.45	0.5

An effective absorption coefficient (equivalent to the experimented process) is defined (α_{eff}^{eq}). This coefficient is 2.2 times higher than that obtained with static tests (considering a low fluence range in both cases), whereas the threshold fluence is 3 times lower. Two assumptions could explain this observation: (a) an incubation effect over at least the 84 first pulses, leading to an increase of the effective absorption coefficient from 5 pulses (table 1) to 84 pulses (table 2), (b) the use of a wider beam, generating a larger amount of ablated material, thus leading to a more pronounced surface shielding.

5. Case study: tube machining

5.1. Experimental conditions

Again, series of laser milling have been performed at the surface of a thin Ta_2O_5 aerogel sample. Holes (between approx. 0.8 mm to 1.2 mm in diameter) have been drilled according to the same machining strategy as explained above (concentric circles, from center to periphery). Then each hole has been longitudinally cut. Half-holes have been observed and their profile measured by SEM.
Profiles are given below. For a better understanding, they have been normalized to the holes entrance diameter (vertical axis expressed in % of variation relative to entrance diameter).

5.2. Operating parameters

Regarding the holes machining, some parameters have been fixed at the beginning of this study. This was the case of linear velocity (5 mm/min), the repetition rate (50 Hz) and the spot geometry (circular in all cases). Besides, in order to keep a reasonable machining time, the choice has been made to limit the number of cuts at 5 or 6.
The variable parameters were the following: laser fluence, spot size, radial overlapping, machining strategy (Z fixed or in motion during the process). A problem arises from their strong interdependence, which tends to complicate the analysis of their individual impact on the hole geometry. However, we attempted a separate analysis thank to separate series of tests. Their impact on the beam profile has been evaluated, up to highlight a nominal set of parameters.

5.3. Influence of the operating parameters

- Pulse energy

For this set of tests, the laser beam has been focused at the sample surface (fixed Z).
Different aspects have been analysed:

- In Fig 3a, the influence of pulse energy on hole profiles has been plotted. The corresponding holes have been obtained with a 130 µm spot size.
- In fig 3b, the maximum hole depth (distance from top to bottom) is shown, sometimes exceeding the sample thickness, for three different spot size (65 µm, 130 µm, 250 µm),
- In fig 3c are plotted the depths at which the diameter variation didn't exceed 100 µm (revealing a taper defect), for three different spot sizes.

So it can be seen that the use of higher pulse energy (150 mJ in that case) is a good way to produce deeper holes (Fig. 3a and 3b). The consequence is a larger amount of micrometric ablated residues we can observe on the inner walls (Fig. 3a).
Moreover, at 150 mJ, the shape remains cylindrical over an increased depth (except for the wider beam - Fig. 3c).

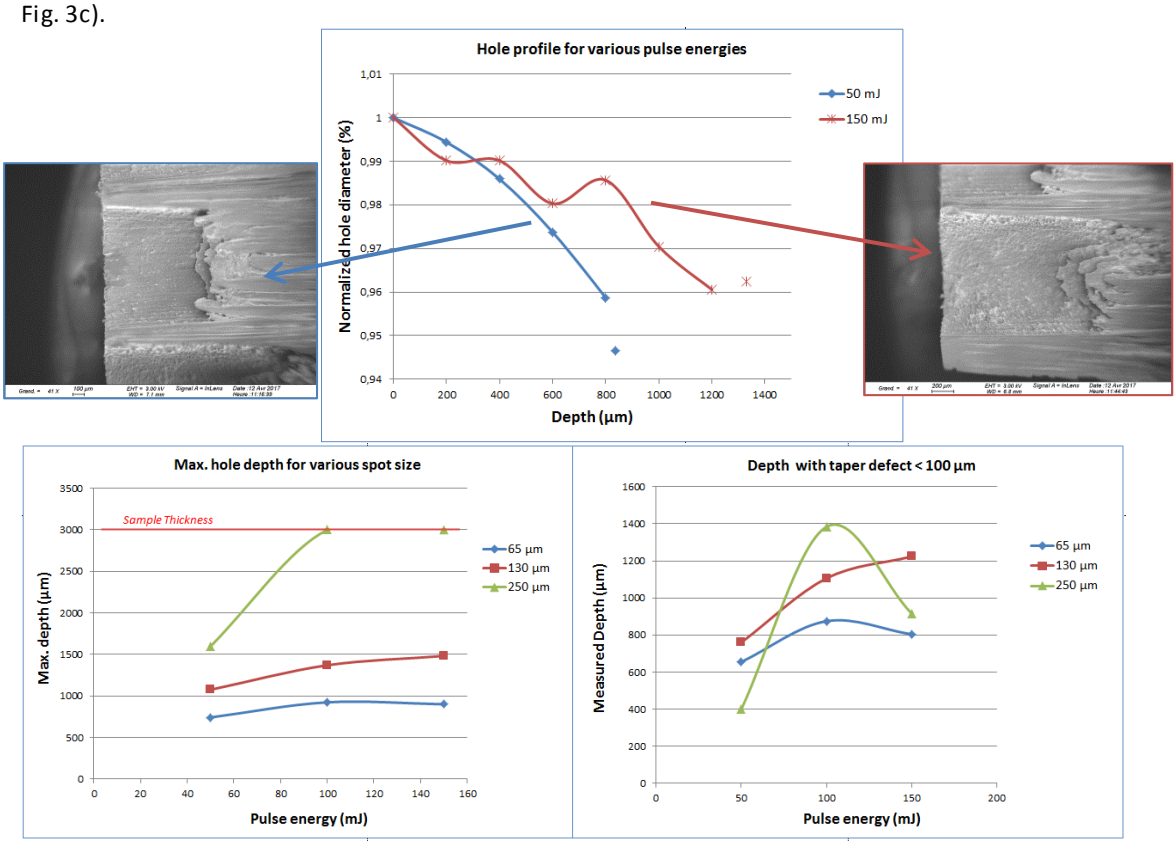

Fig. 3. Dependence to the pulse energy (a) hole profile and SEM hole observation; (b) maximum achievable penetration; (c) depth affected by a hole diameter variation below 100 µm

Measurements show also that the maximal depth tends to saturate with pulse energy (Fig. 3b). In order to overcome this problem, a dynamic focusing can be performed during the machining: it's the Z-scan.

- Z-scan

This series of tests consisted in refocusing the beam thanks to a vertical translation of 300 µm per cut. The impact of this strategy is compared to a fixed Z below (Fig. 4), for pulse energy of 50 mJ.

The influence of a Z-scan is obvious with a large spot (Fig. 4a): the hole is deeper and the shape more cylindrical than at fixed Z. This conclusion is about the same for a smaller spot (Fig. 4b), but the gain is far weaker.
For comparison, we have also reported a profile obtained at fixed Z and 150 mJ (Fig. 4b): even with the use of a pulse energy divided by 3, the maximum depth remains greater with a Z-scan, showing the efficiency of the method. Moreover, a Z-scan is easy to implement in the CNC program, and doesn't affect the overall machining time.

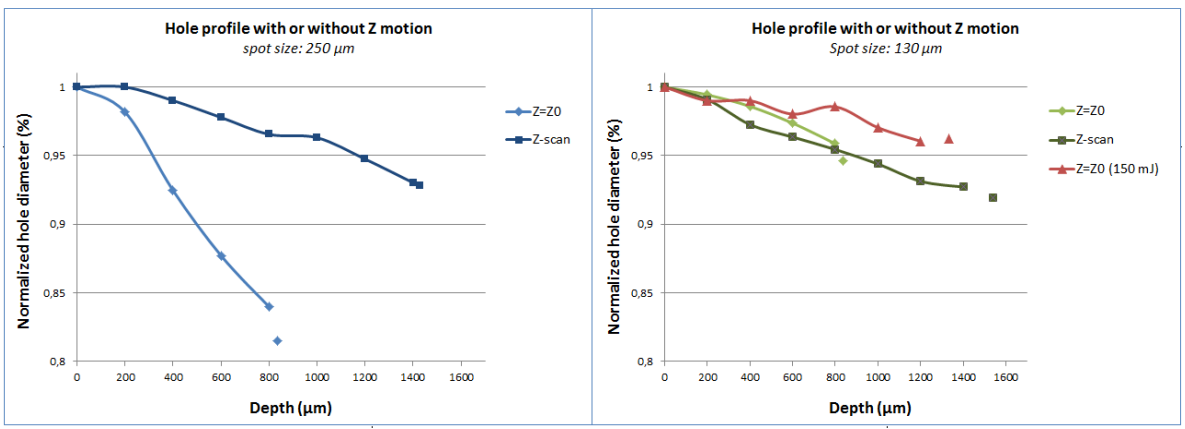

Fig. 4. Influence of a Z-scan on the hole profiles for various spot size (a) 250 µm ; (b) 130 µm

- Spot size

Spot size variation has been performed at fixed Z (Fig. 5a) and Z-scan (Fig. 5b).
In the first case, the use of a larger beam allows to drill a deeper hole (especially with a higher pulse energy, where hole's depth exceeds 3 mm). Conversely, the use of a smaller spot (130 µm) ensures a better cylinder shape (Fig. 5a) and this shape remains stable with pulse energy (Fig 3c), which didn't seem the case with a larger beam (Fig. 3c).
A spot of 130 µm seemed the best compromise for fixed Z, but without significant influence for Z-scan (Fig. 5b).

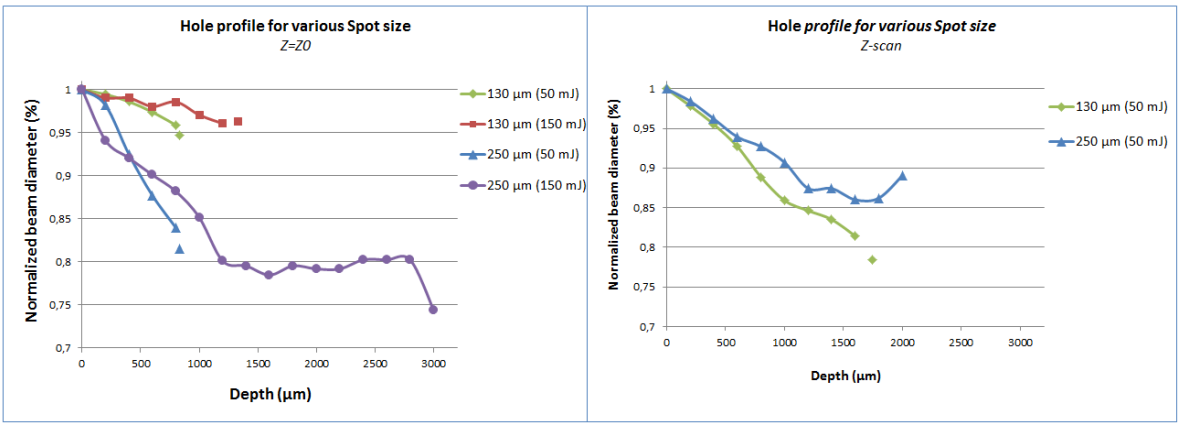

Fig. 5. Influence of spot size on the hole profiles (a) at fixed Z ; (b) in Z-scan

- Spatial (radial) overlapping

This parameter refers to the spatial overlap between two adjacent (concentric) circles. These tests have been performed in Z-scan configuration, with pulse energy of 50 mJ.

As expected, the use of large overlaps deepens holes, but this choice is time-consuming. Anyway, a machining with no overlap will be preferred, leading to a more cylindrical hole (red curve in Fig. 6).

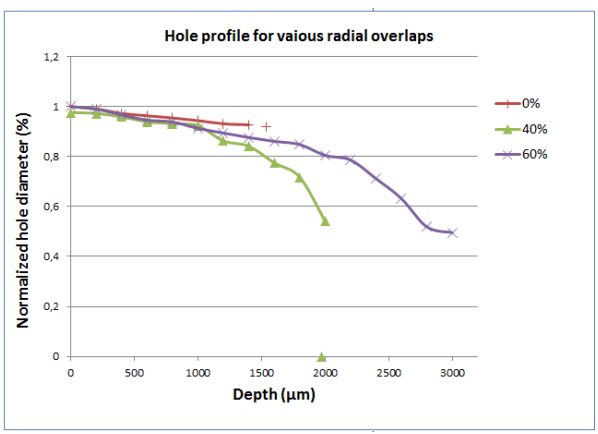

Fig. 6. Influence of the spatial overlap

5.4. Tube machining with the optimum set of parameters

According to the presented results, the most relevant parameters playing a role on the holes' shape and maximum depth are the pulse energy and a dynamic focalization (Z-scan). The other parameters can be considered, but to a lesser degree.

To conclude this study, a tube has been machined according to the following principle:

- Gluing of a bulk sample on a specific holder,
- Classical laser turning (ArF laser) up to obtain a millimetric cylinder,

- Milling of the inner part with the nominal parameters, i.e. by using a circular spot (130 µm in diameter) at pulse energy of 150 mJ and a repetition rate of 50 Hz. The sample motion has been programmed in concentric circles without overlapping, with dynamic Z motion of 300 µm per cut. In order to attempt hole deepening, a number of 10 cuts has been applied.

The final result is shown Fig. 7. This tube features an outer diameter of 1650 µm, an inner diameter of 1375 µm (at the tube entrance) and an inner depth of 2850 µm. The inner diameter decreases along the tube length, but this effect remains moderate: at 1.3 mm from the entrance side, the diameter has decreased by 80 µm.

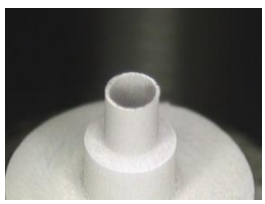

Fig. 7. Final tube, obtained by ArF laser micromachining

6. Conclusion

This paper details a parametric study applied for laser processed Ta_2O_5 aerogels. It shows that, despite a quite low material absorption coefficient, a machining process can be implemented and optimized. Indeed, the process results in the fabrication of a millimetric object of interest for laser-plasma experiments. Today, the main limit is related to the taper defect that has been minimized but not totally annihilated.
This work will continue on a femtosecond laser. The corresponding workstation enables versatility in optical configuration and workpiece motion that should lead to improvements of the taper defect. Moreover, it will be the opportunity to compare abilities of ultrafast regime and UV nanosecond regime to process this material.

References

Ampere, A. et al, 2007, "Recent developments on microablation of glass materials using excimer lasers", Optics and lasers in engineering, 45, 975-992.

Desbiens, J-P, 2007, "ArF excimer laser micromachining of Pyrex, SiC and PTZ for rapid prototyping", Sensors and actuors A, 136, 554-563.

Dyer, P.E., 1996, "Excimer laser ablation of polymers and glasses for grating fabrication", Applied surface science, 96-98, 537-549.

Bourdenet, R., Geoffray, I. et al, 2015, "3D laser-micromachining for targets manufacturing", Proceedings of the Lasers in manufacturing conference (LIM) Munich, Germany, June 2015.

Frederick, C.A et al, 2009, "Fabrication of Ta2O5 aerogel targets for radiation transport experiments using thin film fabrication and laser processing", Fusion science and technology, vol 55, 499-504.

Holland, S. et al, 2014, "Low density material fabrication", 5th Target Fabrication Workshop, St Andrew, Scotland, 6-11/07/2014.

Ihleman, J. et al, 1993,"Excimer laser micromachining", Advances materials for optics and electronics, vol 2, 87-92.

Lippert, T., "Laser application of polymers", 2004, Adv Polym Sci 168:51-246.

S. Ambreen, ND. Pandey, P. Mayer et A. Pandey, 2014, "Characterization and photocatalytic study of tantalum oxide nanoparticles prepared by the hydrolysis of tantalum oxo-ethoxide $Ta_8(\mu_3\text{-}O)_2(\mu\text{-}O)_8(\mu\text{-}OEt)_6(OEt)_{14}$", Beilstein Journal of nanotechnology, 5, 1082-1090.

Urech, L, 2010, "Photoablation of polymer materials", Photochemistry and photophysics of polymer materials, Editor Norman S. Allen, p 541.